Molecular imaging of coronary plaque vulnerability using 18F- fluorocholine PET-MRI in patients with coronary artery disease: validation with optical coherence tomography

Jochem A.J. van der Pol

jochem.vander.pol@mumc.nl

Maastricht University Medical Center

Braim Rahel

VieCuri Medical Centre for Northern Limburg

Yvonne J.M. van Cauteren

Maastricht University Medical Center

Rik P.M. Moonen

Maastricht University Medical Center

Joan G. Meeder

VieCuri Medical Centre for Northern Limburg

Suzanne C. Gerretsen

Maastricht University Medical Center

Mueez Aizaz

Maastricht University Medical Center

Claudia Prieto

King's College London

René M. Botnar

King's College London

Jan Bucerius

University Medicine Goettingen, Georg-August-University

Herman van Langen

VieCuri Medical Centre for Northern Limburg

Joachim E. Wildberger

Maastricht University Medical Center

Robert J. Holtackers

Maastricht University Medical Center

M. Eline Kooi

Maastricht University Medical Center

Research Article

Keywords: fluorocholine, PET-MRI, optical coherence tomography, plaque imaging, atherosclerosis

Posted Date: August 9th, 2024

DOI: https://doi.org/10.21203/rs.3.rs-4686936/v1

Additional Declarations: No competing interests reported.

Abstract

Purpose

^{18}F-fluorocholine is a positron emission tomography (PET) tracer earlier found to be a marker of macrophage content in carotid plaques. We aimed to assess the feasibility of ^{18}F-choline PET-MRI to non-invasively localize vulnerable coronary plaques, using optical coherence tomography (OCT) as reference standard.

Methods

Patients with recent myocardial infarction who were scheduled for a secondary angiography of a non-culprit vessel, underwent ^{18}F-fluorocholine coronary PET-MRI. Subsequently, OCT was performed during the secondary angiography. Maximum target-to-background (TBRmax) values of ^{18}F-fluorocholine uptake were determined in two vessel sections that contained either vulnerable or stable plaques as defined by OCT. The OCT-based definition of a vulnerable plaque was a fibrous cap thickness <70µm. To enhance the detectability of coronary plaques using PET, three different motion-correction strategies were used: multigate respiratory gating motion correction (MRG-MOCO), extended MR-based motion correction (eMR-MOCO), and extended MR-based motion correction with ECG gating (eMR-MOCO-ECG).

Results

Fifteen patients were included in this study, of which eleven entered final analyses. Data of the other four subjects could only be partially analysed. TBRmax values were as follows for three different reconstructions in vulnerable versus stable plaques: MRG-MOCO: mean TBRmax 1.45 vs 1.35, p=0.52; eMR-MOCO mean TBRmax 1.47 vs 1.27, p= 0.26, eMR-MOCO-ECG: mean TBRmax 1.49 vs 1.26, p= 0.21.

Conclusion

^{18}F-fluorocholine uptake in vulnerable atherosclerotic plaques in coronary arteries was not significantly different from uptake in stable plaques even though advanced motion-correction methods were applied. That may be caused by multiple factors, such as small coronary plaque size and remaining cardiac motion.

Introduction

Atherosclerosis is a progressive, chronic, inflammatory disease with systemic manifestations affecting large and medium-sized arteries. As a result, fatty streaks or plaques are formed inside these arteries that can narrow them over time. Such plaques can erode over time or even suddenly rupture, thereby potentially causing a thrombotic occlusion of the vessel and obstructing the blood flow. The majority of myocardial infarctions (MI) are caused by such thrombotic events.[1] Although atherosclerotic plaques

have certain pathological characteristics, such as positive remodelling, micro-calcification, and a large necrotic core, identification of vulnerable plaques remains challenging.[2,3]

Previously, it was shown that implementing cardiac magnetic resonance (CMR) or computed tomography angiography (CTA) in the diagnostic process in NSTEMI patients is a safe gatekeeper for (therapeutic) invasive coronary angiography (ICA).[4] Regardless, the risk of recurrent MI remains approximately 10% within the first year and 5% in each of the subsequent 4 years.[5,6] This is most likely an underestimation, because 17-26% of recurrent plaque ruptures and MI remain clinically silent.[7] The high recurrence rate could be attributable to inaccurate angiographic identification of vulnerable plaques resulting in inadequate treatment.[8-10] The situation is worsened by the fact that vulnerable plaques tend to occur at multiple coronary sites in approximately 40% of the patients.[10] Furthermore, it is known that 'high-risk' lesions that are anatomically unrelated to the initial event are often responsible for recurrent ischemic events.[10,11] Thus, performing angioplasty of only a single lesion may be an insufficient preventive measure.

Non-invasive imaging techniques, such as position emission tomography (PET), have the advantage that they can be used longitudinally and allow studying the natural behaviour of vulnerable plaques. Nowadays, hybrid PET-MRI scanners exist that combine the advantages of molecular imaging using PET with the superior soft tissue contrast of magnetic resonance imaging (MRI).[12] Hybrid PET-MRI also provides a unique opportunity to apply MRI-based respiratory motion correction on both MRI and PET images. Munoz et al. showed that a non-rigid respiratory motion-compensated coronary magnetic resonance angiography approach enabled respiratory motion-correction of the hybrid MRI as well as the PET images. [13]

Among the available radioactive PET tracers, ^{18}F-fluorodeoxyglucose (FDG) is mostly used in oncology but has also proven its value in imaging inflammatory changes of the arterial wall. However, since FDG remains a more unspecific inflammation tracer and has several drawbacks in imaging the coronary arteries, e. g. physiological uptake in the myocardium. Recent evidence suggests that other more specific tracers may be used for metabolic imaging of cell activation, especially in macrophages.[14] Earlier studies demonstrated the feasibility of radiolabeled-choline for imaging atherosclerosis, showing ^{18}F-fluorocholine PET being able to identify the inflammatory regions in symptomatic carotid artery plaques with a significant correlation between tracer uptake and macrophage content on histology.[15]

In contrast to hybrid PET-MRI, optical coherence tomography (OCT) is an invasive imaging technique that is able to provide detailed images of coronary plaques with a resolution ranging from 10 to 20 micrometers, which is approximately 50-100 times higher than what can be achieved using MRI or intravascular ultrasound (IVUS). Due to its superior spatial resolution, OCT can identify a key feature of coronary plaque vulnerability, i.e. the presence of a thin fibrous cap [16]. OCT already proved its usefulness in numerous studies and is therefore considered a reference standard [16-18].

In the present feasibility study, we will investigate whether non-invasive ^{18}F-fluorocholine PET-MRI can be used to identify vulnerable atherosclerotic plaques in the coronary arteries. We will test the hypothesis that vulnerable plaques show a locally increased uptake of ^{18}F-fluorocholine on PET-MRI compared to stable plaques using invasive OCT as reference standard.

Methods

Study population

Subjects who presented with non-ST elevation myocardial infarction (NSTEMI) at the VieCuri hospital in Venlo, underwent percutaneous coronary intervention (PCI) of the culprit vessel, and were diagnosed with multivessel coronary artery disease and subsequently scheduled for a second PCI, were recruited for study participation. NSTEMI was defined as ischemic symptoms with elevated cardiac enzymes (Troponin T/I, creatin kinase-MB), however, in absence of ST-segment elevations in the ECG. Exclusion criteria were conservatively managed patients not scheduled for PCI, ongoing severe ischaemia requiring immediate PCI, hemodynamic instability, severe heart failure (Killip Class ≥ III), chest pain highly suggestive of non-cardiac origin, suspicion or evidence of acute aortic dissection, acute pulmonary embolism, acute pericarditis, life threatening arrhythmias at the cardiac emergency department or before presentation, tachycardia (>100bpm), angina pectoris secondary to anaemia, untreated hyperthyroidism or severe hypertension (>200/110 mmHg), moderate to severe aortic or mitral valve stenosis, pregnancy, breast feeding and contra-indications for MRI, including metal implants, cardiac implantable devices, claustrophobia, renal failure and allergy to gadolinium-containing contrast media. This study was approved by the local ethics committee (METC162043 / NL58752.068.16) and conducted according to the declarations of Helsinki. All subjects were 18 years or older and provided written informed consent.

PET-MR imaging

After the first PCI procedure in the acute setting and within 72 hours of the scheduled second PCI procedure, hybrid PET-MRI imaging was performed on a fully-integrated combined 3 Tesla PET-MRI system (Biograph mMR; Siemens Healthineers, Erlangen, Germany) at the Maastricht University Medical Centre. Subjects were scanned in headfirst supine position using a 6-channel body matrix and the 12-channel spine radiofrequency coils. First, an MRI-based attenuation map (μ-map) was acquired during an end-expiration breath-hold.[18] Relevant parameters of this Dixon-based μ-map include: field-of-view (FOV) = 599 x 271 x 408 mm^3, acquired resolution = 2.1 x 2.1 x 2.6 mm^3, flip angle = 10°, repetition time (TR) = 3.85 msec, and echo time (TE) =2.46 msec. Following the μ-map acquisition, the ^{18}F-fluorocholine PET tracer (BV Cyclotron VU, Amsterdam, the Netherlands) was intravenously injected with a dose of 4 MBq/kg (up to a maximum dose of 360 MBq). Five minutes after PET tracer injection, a static list-mode PET acquisition was started while the respiratory signal was recorded using the respiratory belt. Previous research in the carotid artery showed stable FCH uptake from 10 minutes until 1 hour after injection in both symptomatic and asymptomatic carotid artery, as well as in vascular background. [15]

Simultaneously during PET acquisition, coronary MR angiography (CMRA) was performed 2 minutes after an intravenous contrast agent injection of 0.2 mmol/kg gadobutrol (Gadovist; Bayer Pharmaceuticals, Berlin, Germany), up to a maximum of 20 mmol. A 3D spoiled gradient-echo sequence with a fully sampled golden-step Cartesian trajectory with spiral profile ordering was used. Relevant sequence parameters include: FOV = 304 × 304 × 104 mm^3, acquired resolution = 1.0 × 1.0 × 2.0 mm^3, flip angle = 15°, TR = variable based on heart rate, TE = 1.7 msec, acquisition window ranging between 90 to 130 msec. Three-lead ECG registration was performed to allow for cardiac motion gating. Every heartbeat, just before each acquisition window, a 2D image navigator (iNAV) was acquired which provides a low-resolution image of the heart in coronal view to allow for subsequent motion correction. Details of this sequence have been previously described. [19]

OCT imaging

Within 72 hours after the hybrid PET-MRI scan, during the planned second PCI procedure at the VieCuri hospital in Venlo, OCT imaging of the secondary pathological vessel was performed before potential stent placement. Before entry in the coronary artery, an intracoronary injection of 100 to 200 µg nitroglycerine was provided. The tip of the OCT catheter (Dragonfly intravascular imaging catheter, St. Jude Medical, St. Paul, MN, USA) was then placed at least 5 mm distal to the distal edge of the lesion. While obtaining optimal blood clearance by flushing the coronary artery with contrast agent using an automated pump, an automatic pullback through the lesion was initiated, covering at least 5 mm of the proximal and distal parts of the vessel.

Image reconstruction

PET image reconstruction was performed with e7 Tools (Siemens Healthineers, Erlangen, Germany) using the ordinary Poisson-ordered subset expectation maximization (OP-OSEM) algorithm with 3 iterations and 21 subsets. Images were reconstructed with a voxel size of 2.08 x 2.08 x 2.03 mm^3 and a matrix size of 344 x 344 x 127. For PET attenuation correction, MR-based Dixon µ-maps were used that provided separation between air, lung, fat, and soft tissue. To make up for the smaller FOV of MRI with respect to PET, the maximum likelihood reconstruction of attenuation and activity (MLAA) approach was utilized.

For CMRA motion correction,motion in the left-right (LR) and feet-head (FH) direction is estimated for each heartbeat using the apex of the heart in the iNAV images. Based on the amplitude in the FH direction, CMRA data is allocated to four respiratory phases or bins. k-space data inside each bin is corrected to the centre of the bin using the FH and LR position estimates derived from the iNav. Next, each bin is reconstructed. Using the end-expiration bin as a reference, respiratory non-rigid deformation fields are generated which are subsequently applied to transform each bin to the end-expiration position generating the motion-compensated CMRA image.[19]

Three different motion correction strategies were available to correct the PET datasets for respiratory motion: 1) Multiphase respiratory gating motion correction (MRG-MOCO), where motion correction was based solely on the respiratory belt signal as acquired during the entire PET acquisition. Only the PET data acquired during the end-expiration phase were used for image reconstruction. 2) Extended MR-based MOCO (eMR-MOCO), where both the iNav respiratory signal (as described earlier, but only available during ~ 9 minutes of CMRA imaging) and the respiratory belt signal (available entire PET acquisition) are used.[20] The time window for which both the iNav respiratory signal and respiratory belt signal was collected, was used to ensure that the binning of PET data on the iNav signal closely matches the binning on the respiratory belt signal by adjusting binning thresholds. These thresholds are then extended for respiratory motion correction of the complete duration of the PET scan. Each bin was reconstructed and combined with other bins using iNav-based motion fields to a reference position to create a respiratory motion-corrected dataset. 3) Finally, eMR-MOCO-ECG applied the combination of eMR-MOCO (strategy 2) and ECG-based cardiac gating to mitigate cardiac motion as well. Only PET data acquired during the end-diastolic phase, which was derived from CMRA sequence ,was used for eMR-MOCO-ECG reconstruction, other data was discarded.

Image analysis

The OCT data was analysed by an independent core lab (LIMIC Medical, Ridderkerk, the Netherlands) where fibrous cap thickness was determined in all plaques. Plaque vulnerability was defined as a plaque with a thin fibrous cap of ≤ 70 μm.[16] PET imaging was then co-registered with the CMRA images and analysed using MIM Vista (MIMsoftware, Cleveland, OH, USA). The OCT slice position of the vulnerable plaque was located on the 3D MRI, using vessel side branches as landmarks, by a cardiologist (BR) and nuclear medicine physician (JP). A volume of interest (VOI) was defined around the pathological vessel section. In the same vessel, a control lesion with a thick fibrous cap was selected on OCT, pinpointed on the MRI, and analysed using the same approach as described for the target lesion. The maximum standardized uptake value (SUVmax) was measured in both the target and control lesions. Target-to-background ratios (TBR) were calculated, by dividing SUVmax values of the target and control lesions by the mean standardized uptake value (SUVmean) of the blood pool in the left atrium.

Statistics

Differences in TBR ratios between vulnerable and stable plaques were tested by paired Student’s t-test (normally distributed data) or Wilcoxon signed-rank test (non-normally distributed data). Normality of data was tested using the Shapiro-Wilk test. The correlation between TBRmax and minimal fibrous cap thickness for the combined target and reference lesions was assessed using Spearman’s rho correlation coefficient for each PET reconstruction. All statistical analyses and plot generations were performed using RStudio (Integrated Development Environment for R, version 1.4.1103, Boston MA, USA). Two-tailed values of $p < 0.05$ were considered significant.

Results

A total of 15 patients were included for this study. One patient was excluded from final analysis due to PET tracer extravasation. The baseline characteristics of the remaining 14 patients are described in **Table 1**. Three patients could only be partially analysed due to the following reasons: 1) CMRA with nondiagnostic image quality due to artifacts (excluded for TBRmax eMR-MOCO and eMR-MOCO-ECG analyses), 2) no coronary reference lesion available (excluded for target versus reference TBRmax comparison), and 3) failure to produce all PET respiratory gating reconstructions (excluded for eMR-MOCO and eMR-MOCO-ECG analyses). All analysed patients had a vessel section with a fibrous cap thinner than 70 µm. **Figure 1** shows imaging examples of the acquired PET-MRI and OCT imaging.

No significant difference between TBRmax values of the vulnerable versus the stable lesions for MRG-MOCO, eMR-MOCO and eMR-MOCO-ECG were found (MRG-MOCO: mean TBRmax 1.45 vs 1.35, p=0.52; eMR-MOCO: 1.47 vs 1.27, p= 0.26; eMR-MOCO-ECG: 1.49 vs 1.26, p= 0.21). Boxplots and dot plots of vulnerable versus stable plaque TBRmax values for the different PET reconstructions are shown in **Figure 2**.

No significant correlation between TBRmax and minimal fibrous cap thickness was found for each of the PET reconstructions (MRG-MOCO: -0.034, p=0.87; eMR-MOCO: -0.057, p=0.80; and eMR-MOCO-ECG: -0.036, p=0.87). Scatterplots of the TBRmax and minimal fibrous cap thickness of the combined vulnerable and stable plaques for each PET reconstruction are shown in **Figure 3**.

A comparison of the three used PET imaging reconstructions is shown in **Figure 4**. A difference in noise can be visually appreciated between the different reconstructions, where MRG-MOCO reconstruction yields more noise than both eMR-MOCO and eMR-MOCO-ECG.

Discussion

To the best of our knowledge, this is the first study that investigates the feasibility to identify vulnerable coronary plaques with non-invasive ^{18}F-fluorocholine PET. Coronary imaging is challenging due to inherent motion artefacts caused by both respiratory and cardiac motion. To correct for these motion artifacts, advanced hybrid PET-MRI respiratory motion correction as well as cardiac gating methods were applied in different combinations. Nevertheless, no significant differences were found in ^{18}F-fluorocholine PET uptake between vulnerable and stable coronary plaques as classified by invasive OCT imaging as reference standard.

The use of hybrid PET-MRI in the present study allows for nonrigid respiratory motion correction in our patient population. This PET-MRI reconstruction method allowed to estimate translational motion from a low-resolution 2D MR image navigator (iNav) acquired each heartbeat and to subsequently apply 3D nonrigid respiratory motion correction between different respiratory bins from the CMRA data. In contrast, respiratory motion correction methods in PET-CT for correction of pulmonary and upper abdominal motion artifacts, are only correcting in craniocaudal direction. This important advantage of

hybrid PET-MRI imaging potentially provides a non-invasive method for analysing the coronary arteries. Another advantage is that molecular imaging on PET can be combined with functional ischemia imaging on MRI.

In contrast to ^{18}F-FDG PET imaging, which has significant drawbacks for coronary imaging, radiolabeled-choline is highly taken up in activated macrophages and was hypothesized to be an alternative, more specific, tracer for imaging plaque inflammation.[15] Initial murine and rabbit models of atherosclerosis revealed a significantly higher uptake of radiolabeled-choline in inflamed atherosclerotic plaques in comparison to healthy vessel wall.[21-23] This rapid uptake of radiolabeled-choline in plaque macrophages seems to be linked to the upregulation of choline transporters on the cell surface, similar to that observed in macrophages from other inflammatory conditions.[14, 22] There are three published reports that retrospectively analysed choline PET in diagnosis of prostate cancer, and described a higher presence of the tracer within the atherosclerotic vessel walls.[24-26] For obvious reasons, no comparison with the gold standard, histology, has been made in these studies. Our own group earlier investigated vascular wall inflammation in a prospective study that compared ^{18}F-fluorocholine uptake to macrophage content on histology, represented by CD68+ plaque content, in a patient population of symptomatic carotid artery stenosis.[15] That study showed a positive correlation between ^{18}F-fluorocholine uptake and macrophage content, as well as higher uptake in the ipsilateral versus contralateral carotid vessel wall.

An explanation for the lack of ^{18}F-fluorocholine uptake in vulnerable coronary plaques in the current study could be related to the small size of coronary plaques, compared to larger carotid artery lesions studied earlier. A certain minimum amount of tracer needs to accumulate in a plaque in order to be detected by PET. Subvoxel size of plaques does not rule out detection, but the partial volume effect can negate detectability. Studies with other tracers, notably ^{18}F-sodiumfluoride (^{18}F-NaF), revealed increased tracer uptake in culprit versus non-culprit coronary plaques of patients with myocardial infarction.[27] Interestingly, this study also showed that patients with ^{18}F-NaF positive plaques in a stable angina cohort had higher ^{18}F-NaF activity when compared to those with myocardial infarction. The patients with stable angina were older and therefore may have had a more extensive plaque burden. Thus, not only the vulnerability but also the size of the plaque determines the TBRmax value.

When investigating coronary artery plaques, no coronary artery specimens can be obtained to correlate PET outcomes to histological findings. In our study, invasive OCT imaging was used as reference standard to provide detailed images of coronary plaques with a resolution ranging from 10 to 20 μm. This is approximately 50-100 times higher than what can be achieved using MRI or intravascular ultrasound (IVUS), and OCT has been well validated in numerous studies.[16,17,28-30] The OCT parameter that we used to define a vulnerable plaque was the presence of a thin fibrous cap, since rupture of such a cap is the main underlying cause of myocardial infarction. We used a threshold of a cap thickness of less than 70 μm for a vulnerable plaque in line with previous studies.[31] While

pathologists define a thin fibrous cap using a cut-off value of < 65 μm,[32] for OCT one should choose a slightly higher threshold to take into account tissue shrinkage during histological processing.[33]

The anatomical correlation of the plaques on OCT and PET relied on visually comparing vascular anatomy as displayed on angiographical imaging to the coronary MR angiography images. By carefully selecting a segment with stable plaque, sufficiently distant away from vulnerable plaques, we ensured that the stable plaque VOI did not include a section of vulnerable plaque. We also made sure that the entire plaque was included in the VOI. The advantage of TBRmax is that this parameter is not influenced by the VOI size, as long as no other ^{18}F-fluorocholine avid structures are included. Therefore, the current negative results, cannot be explained by high uptake in stable plaques. Theoretically, a conebeam CT acquired using a state-of-the-art angiographic gantry could be better suited to co-registrate the OCT pullback trajectory with the PET images. On the other hand, such a technique would lead to extra radiation exposure.

Finally, a practical limitation concerning the analysis of ^{18}F-fluorocholine uptake in coronary vessels is intense liver uptake, obscuring any vascular uptake located close to the liver due to spill over of liver activity. This mostly affects the distal right coronary artery, where lumen and plaques tend to be smaller and are already inherently more challenging for PET imaging in general. In our patient population, however, all vulnerable and stable plaques that were analysed were in regions not susceptible to activity overspill from the liver. Another limitation of the study is the small sample size since the study was conceived to establish proof of principle.

Conclusion

PET-MRI with ^{18}F-fluorocholine, using advanced respiratory non-rigid motion correction with or without cardiac gating, did not show significantly higher uptake in vulnerable plaques compared to stable plaques using OCT as reference standard. These findings in the coronary arteries differ from previous results in the carotid arteries, where more uptake in symptomatic lesions was observed. Multiple inherent factors, such as small coronary plaque size and cardiac movement, may hamper visualization of coronary macrophage plaque content through ^{18}F-fluorocholine binding.

Statements and declarations

Trial registration number:

NCT03252990 (ClinicalTrials.gov)

NL58752.068.16 (Dutch Medical Ethical Committee registration number)

Acknowledgements

We are grateful for all assistance in OCT analysis offered by Jurgen Ligthart (Limic Medical).

The authors would like to acknowledge Jurgen Ligthart (LIMIC Medical) for his assistance with the OCT analysis.

Funding

This project was funded by the Academic Fund of the VieCuri hospital and Maastricht University Medical Center, and the Weijerhorst foundation (Stichting de Weijerhorst).

Competing interests

The authors Jochem A.J. van der Pol, Braim Rahel, Yvonne J.M. van Cauteren, Rik P.M. Moonen, Joan G. Meeder, Suzanne C. Gerretsen, Mueez Aizaz, Claudia Prieto, René M. Botnar, Jan Bucerius, Herman van Langen, Robert J. Holtackers and Eline M. Kooi declare no conflicts of interest. Joachim. E. Wildberger reports institutional grants by Bard, Bayer, Boston, Brainlab, GE, Philips and Siemens outside of the submitted work. He reports funding via speakers bureau by Bayer, Siemens, outside of the submitted work. Jan Bucerius reports institutional funding from the International Atomic Energy Agency (IAEA) in the context of the "PIAF"-trial (core lab), outside of the submitted work.

Author contributions

Braim Rahel, Joan Meeder, Robert J. Holtackers, M. Eline Kooi, Jochem A.J. van der Pol, Jan Bucerius and Joachim E. Wildberger contributed to the study conception and design. Patient inclusion was performed by Braim Rahel and Yvonne J.M. van Cauteren. Material preparation, data collection and analyses were performed by Braim Rahel, Yvonne J.M. van Cauteren, Robert J. Holtackers, Mueez Aizaz, Rik P.M. Moonen, Herman van Langen, M. Eline Kooi, Suzanne C. Gerretsen and Jochem A.J. van der Pol. The first draft of the manuscript was written by Jochem A.J. van der Pol, with contributions in methods by Braim Rahel, Rik Moonen, Mueez Aizaz and Robert J. Holtackers. All authors commented and critically reviewed the manuscript. Tables and figures were prepared by Jochem A.J. van der Pol. All authors read and approved the final manuscript.

Ethics approval

This study was performed in line with the principles of the Declaration of Helsinki. Approval was granted by the local Ethics Committee of Maastricht University (Registration number NL58752.068.16).

Data availability

Datasets generated and analysed during current study are available from the corresponding author on reasonable request.

References

1. Virmani R, Kolodgie FD, Burke AP, Farb A, Schwartz SM (2000) Lessons from sudden coronary death: a comprehensive morphological classification scheme for atherosclerotic lesions. Arterioscler Thromb Vasc Biol 20:1262-75. doi:10.1161/01.atv.20.5.1262.
2. Finn AV, Nakano M, Narula J, Kolodgie FD, Virmani R (2010) Concept of vulnerable/unstable plaque. Arterioscler Thromb Vasc Biol 30:1282-92. doi:10.1161/ATVBAHA.108.179739.
3. Dweck MR, Maurovich-Horvat P, Leiner T, Cosyns B, Fayad ZA, Gijsen FJH, et al. (2020) Contemporary rationale for non-invasive imaging of adverse coronary plaque features to identify the vulnerable patient: a Position Paper from the European Society of Cardiology Working Group on Atherosclerosis and Vascular Biology and the European Association of Cardiovascular Imaging. Eur Heart J Cardiovasc Imaging 21:1177-83. doi:10.1093/ehjci/jeaa201.
4. Smulders MW, Kietselaer B, Wildberger JE, Dagnelie PC, Brunner-La Rocca HP, Mingels AMA, et al. (2019) Initial Imaging-Guided Strategy Versus Routine Care in Patients With Non-ST-Segment Elevation Myocardial Infarction. J Am Coll Cardiol 74:2466-77. doi:10.1016/j.jacc.2019.09.027.
5. Cutlip DE, Chhabra AG, Baim DS, Chauhan MS, Marulkar S, Massaro J, et al. (2004) Beyond restenosis: five-year clinical outcomes from second-generation coronary stent trials. Circulation 110:1226-30. doi:10.1161/01.CIR.0000140721.27004.4B.
6. Glaser R, Selzer F, Faxon DP, Laskey WK, Cohen HA, Slater J, et al. (2005) Clinical progression of incidental, asymptomatic lesions discovered during culprit vessel coronary intervention. Circulation 111:143-9. doi:10.1161/01.CIR.0000150335.01285.12.
7. Schelbert EB, Cao JJ, Sigurdsson S, Aspelund T, Kellman P, Aletras AH, et al. (2012) Prevalence and prognosis of unrecognized myocardial infarction determined by cardiac magnetic resonance in older adults. JAMA 308:890-6. doi:10.1001/2012.jama.11089.
8. Buffon A, Biasucci LM, Liuzzo G, D'Onofrio G, Crea F, Maseri A (2002) Widespread coronary inflammation in unstable angina. N Engl J Med 347:5-12. doi:10.1056/NEJMoa012295.
9. Davies MJ, Thomas A (1984) Thrombosis and acute coronary-artery lesions in sudden cardiac ischemic death. N Engl J Med 310:1137-40. doi:10.1056/NEJM198405033101801.
10. Goldstein JA, Demetriou D, Grines CL, Pica M, Shoukfeh M, O'Neill WW (2000) Multiple complex coronary plaques in patients with acute myocardial infarction. N Engl J Med 343:915-22. doi:10.1056/NEJM200009283431303.
11. Stone GW, Maehara A, Lansky AJ, de Bruyne B, Cristea E, Mintz GS, et al. (2011) A prospective natural-history study of coronary atherosclerosis. N Engl J Med 364:226-35. doi:10.1056/NEJMoa1002358.
12. Aizaz M, Moonen RPM, van der Pol JAJ, Prieto C, Botnar RM, Kooi ME (2020) PET/MRI of atherosclerosis. Cardiovasc Diagn Ther 10:1120-39. doi:10.21037/cdt.2020.02.09.
13. Munoz C, Neji R, Cruz G, Mallia A, Jeljeli S, Reader AJ, et al. (2018) Motion-corrected simultaneous cardiac positron emission tomography and coronary MR angiography with high acquisition efficiency. Magn Reson Med 79:339-50. doi: 10.1002/mrm.26690.

14. Wyss MT, Weber B, Honer M, Spath N, Ametamey SM, Westera G, et al. (2004) 18F-choline in experimental soft tissue infection assessed with autoradiography and high-resolution PET. Eur J Nucl Med Mol Imaging 31:312-6. doi:10.1007/s00259-003-1337-4.
15. Voo S, Kwee RM, Sluimer JC, Schreuder FH, Wierts R, Bauwens M, et al. (2016) Imaging Intraplaque Inflammation in Carotid Atherosclerosis With 18F-Fluorocholine Positron Emission Tomography-Computed Tomography: Prospective Study on Vulnerable Atheroma With Immunohistochemical Validation. Circ Cardiovasc Imaging 9. doi:10.1161/CIRCIMAGING.115.004467.
16. Sinclair H, Bourantas C, Bagnall A, Mintz GS, Kunadian V (2015) OCT for the identification of vulnerable plaque in acute coronary syndrome. JACC Cardiovasc Imaging 8:198-209. doi:10.1016/j.jcmg.2014.12.005.
17. Bezerra HG, Costa MA, Guagliumi G, Rollins AM, Simon DI (2009) Intracoronary optical coherence tomography: a comprehensive review clinical and research applications. JACC Cardiovasc Interv 2:1035-46. doi:10.1016/j.jcin.2009.06.019.
18. Majeed K, Bellinge JW, Butcher SC, Alcock R, Spiro J, Playford D, et al. (2021) Coronary (18)F-sodium fluoride PET detects high-risk plaque features on optical coherence tomography and CT-angiography in patients with acute coronary syndrome. Atherosclerosis 319:142-8. doi:10.1016/j.atherosclerosis.2020.12.010.
19. Munoz C, Kunze KP, Neji R, Vitadello T, Rischpler C, Botnar RM, et al. (2018) Motion-corrected whole-heart PET-MR for the simultaneous visualisation of coronary artery integrity and myocardial viability: an initial clinical validation. Eur J Nucl Med Mol Imaging 45:1975-86. doi:10.1007/s00259-018-4047-7.
20. Aizaz M, van der Pol JAJ, Schneider A, Munoz C, Holtackers RJ, van Cauteren Y, et al. (2024) Extended MRI-based PET motion correction for cardiac PET-MRI. Eur J Nucl Med Mol Imaging Physics (in press).
21. Laitinen IE, Luoto P, Nagren K, Marjamaki PM, Silvola JM, Hellberg S, et al. (2010) Uptake of 11C-choline in mouse atherosclerotic plaques. J Nucl Med 51:798-802. doi:10.2967/jnumed.109.071704.
22. Matter CM, Wyss MT, Meier P, Spath N, von Lukowicz T, Lohmann C, et al. (2006) 18F-choline images murine atherosclerotic plaques ex vivo. Arterioscler Thromb Vasc Biol 26:584-9. doi:10.1161/01.ATV.0000200106.34016.18.
23. Ogawa M, Ishino S, Mukai T, Asano D, Teramoto N, Watabe H, et al. (2004) (18)F-FDG accumulation in atherosclerotic plaques: immunohistochemical and PET imaging study. J Nucl Med 45:1245-50.
24. Bucerius J, Schmaljohann J, Bohm I, Palmedo H, Guhlke S, Tiemann K, et al. (2008) Feasibility of 18F-fluoromethylcholine PET/CT for imaging of vessel wall alterations in humans--first results. Eur J Nucl Med Mol Imaging 35:815-20. doi:10.1007/s00259-007-0685-x.
25. Forster S, Rominger A, Saam T, Wolpers S, Nikolaou K, Cumming P, et al. (2010) 18F-fluoroethylcholine uptake in arterial vessel walls and cardiovascular risk factors: correlation in a PET-CT study. Nuklearmedizin 49:148-53. doi:10.3413/nukmed-0299.

26. Kato K, Yonetsu T, Kim SJ, Xing L, Lee H, McNulty I, et al. (2012) Nonculprit plaques in patients with acute coronary syndromes have more vulnerable features compared with those with non-acute coronary syndromes: a 3-vessel optical coherence tomography study. Circ Cardiovasc Imaging 5:433-40. doi:10.1161/CIRCIMAGING.112.973701.
27. Joshi NV, Vesey AT, Williams MC, Shah AS, Calvert PA, Craighead FH, et al. (2014) 18F-fluoride positron emission tomography for identification of ruptured and high-risk coronary atherosclerotic plaques: a prospective clinical trial. Lancet 383:705-13. doi:10.1016/S0140-6736(13)61754-7.
28. Celeng C, Takx RA, Ferencik M, Maurovich-Horvat P (2016) Non-invasive and invasive imaging of vulnerable coronary plaque. Trends Cardiovasc Med 26:538-47. doi:10.1016/j.tcm.2016.03.005.
29. Ferrante G, Presbitero P, Whitbourn R, Barlis P (2013) Current applications of optical coherence tomography for coronary intervention. Int J Cardiol 165:7-16. doi:10.1016/j.ijcard.2012.02.013.
30. Terashima M, Kaneda H, Suzuki T (2012) The role of optical coherence tomography in coronary intervention. Korean J Intern Med 27:1-12. doi:10.3904/kjim.2012.27.1.1.
31. Tanaka A, Imanishi T, Kitabata H, Kubo T, Takarada S, Tanimoto T, et al. (2008) Morphology of exertion-triggered plaque rupture in patients with acute coronary syndrome: an optical coherence tomography study. Circulation 118:2368-73. doi:10.1161/CIRCULATIONAHA.108.782540.
32. Virmani R, Burke AP, Farb A, Kolodgie FD (2006) Pathology of the vulnerable plaque. J Am Coll Cardiol 47:C13-8. doi:10.1016/j.jacc.2005.10.065.
33. Tearney GJ, Regar E, Akasaka T, Adriaenssens T, Barlis P, Bezerra HG, et al. (2012) Consensus standards for acquisition, measurement, and reporting of intravascular optical coherence tomography studies: a report from the International Working Group for Intravascular Optical Coherence Tomography Standardization and Validation. J Am Coll Cardiol 59:1058-72. doi:10.1016/j.jacc.2011.09.079.

Table

Table 1 Baseline patient characteristics.

Age [years]	63.1 (10.3)
Gender (female; n,%)	3 (21.4)
Weight [kg]	81.3 (12.0)
Systolic blood pressure [mmHg]	135.2 (22.7)
Diastolic blood pressure [mmHg]	72.4 (11.7)
Hemoglobin [mmol/L]	8.5 (1.1)
LDL-cholesterol [mmol/l]	3.2 (1.6)
HDL-cholesterol [mmol/L]	1.1 (0.27)
Total cholesterol [mmol/L]	4.7 (2.0)
Triglyceride [mmol/L]	1.5 (0.6)
Hypertension (n,%)	6 (42.9)
Diabetes mellitus (n,%)	2 (14.3)
Hypercholesterolemia (n,%)	6 (42.9)
Obesity (n,%)	4 (28.6)
Smoking (n,%)	
Never smoked	3 (21.4)
Former smoker	4 (28.6)
Quit smoking during current hospitalization	5 (35.7)
Still smoking	2 (14.3)
History of ischemic heart disease (n,%)	1 (7.1)

All data are indicated as mean (standard deviation), unless indicated otherwise

Figures

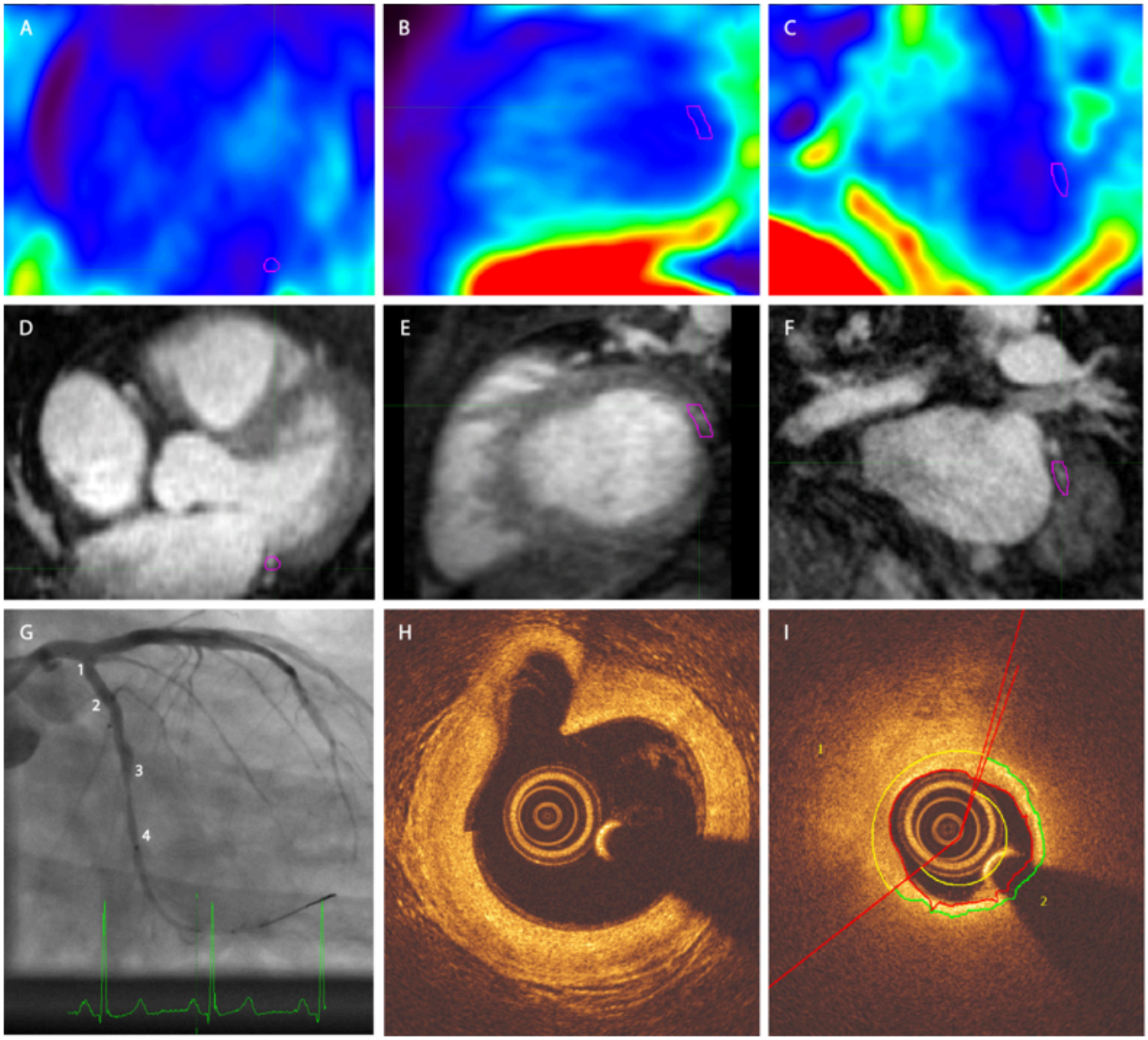

Figure 1

Exemplary PET-MRI and OCT image of one patient. A-C: axial, sagittal and coronary PET. D-F: axial, sagittal and coronary MRI, G: Angiography. Numbers 1-4 represent four different angiographical landmarks to correlate with OCT. A significant stenosis is present between landmarks 3 and 4. H: OCT image corresponding to landmark 1, a large bifurcating vessel can be distinguished in the left upper quadrant of the image; I: OCT image in the region of the stenosis as displayed in panel G. The vessel segment between 2 and 3 contains a plaque with a thin cap on OCT analysis. The purple VOI in panels A-F delineates the target plaque in the left circumflex artery of this patient. No increased tracer uptake was visually detectable in the coronary arteries.

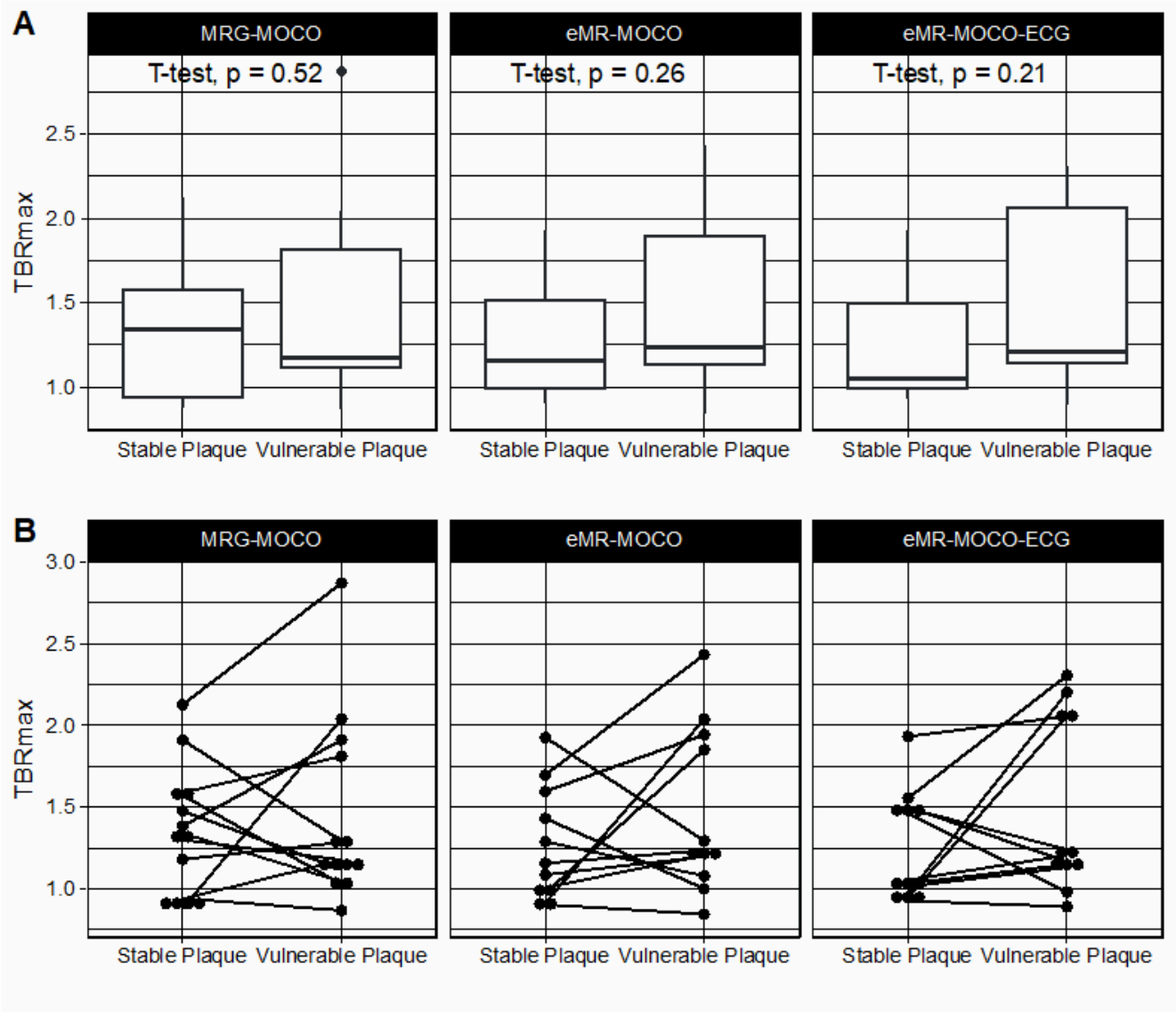

Figure 2

Boxplots (A) and dot plots (B) of TBRmax values of target and reference lesions. No statistically significant differences were found. The lower and upper hinges of the boxplots represent 25th and 75th percentiles respectively, whisker endpoints represent minimum and maximum non-outlying values.

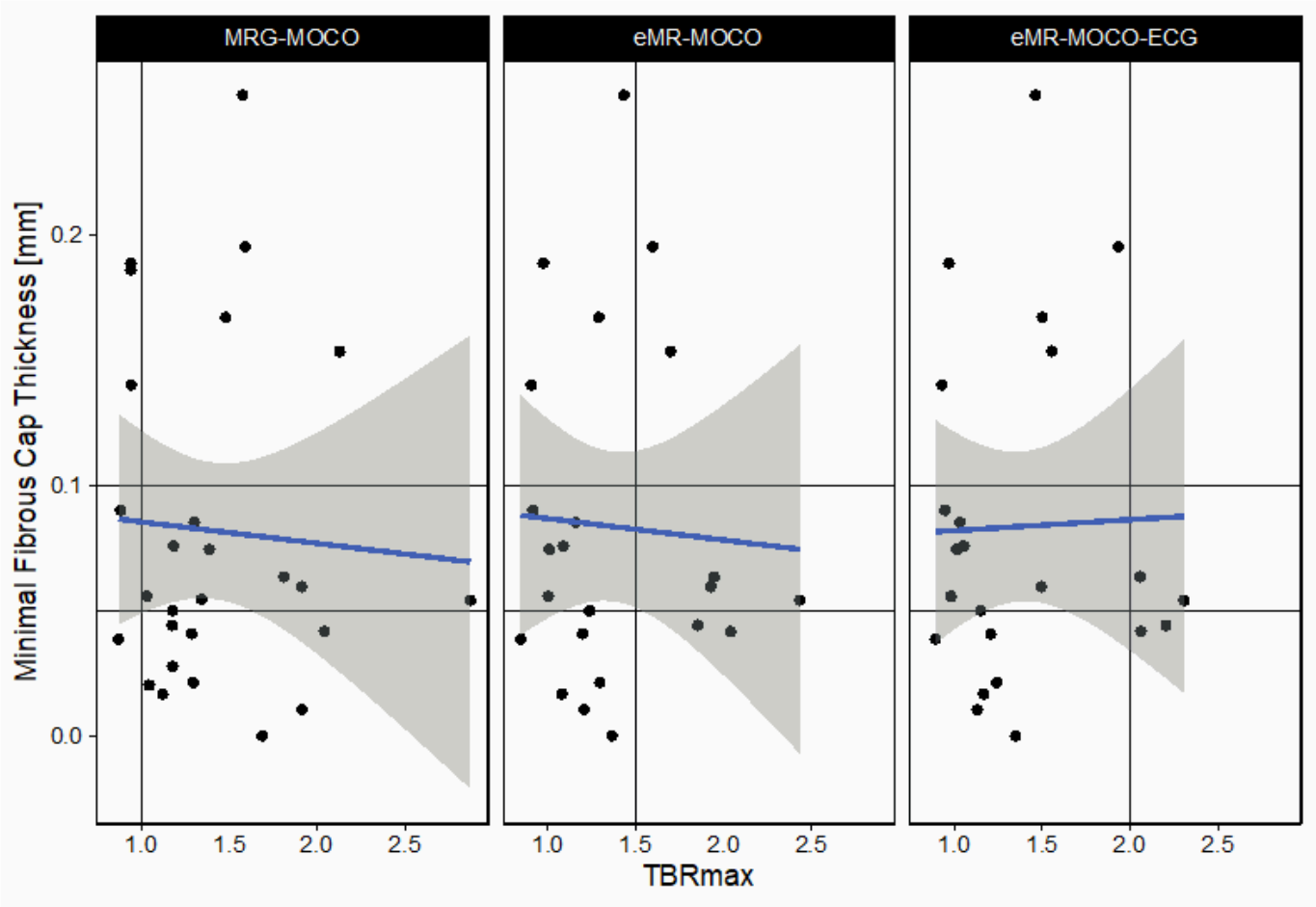

Figure 3

TBRmax values plotted versus Minimal Fibrous Cap Thickness for three different reconstruction methods. No correlation is observed between the TBRmax and the fibrous cap thickness. Regression lines are plotted in blue, with standard error interval displayed as grey area.

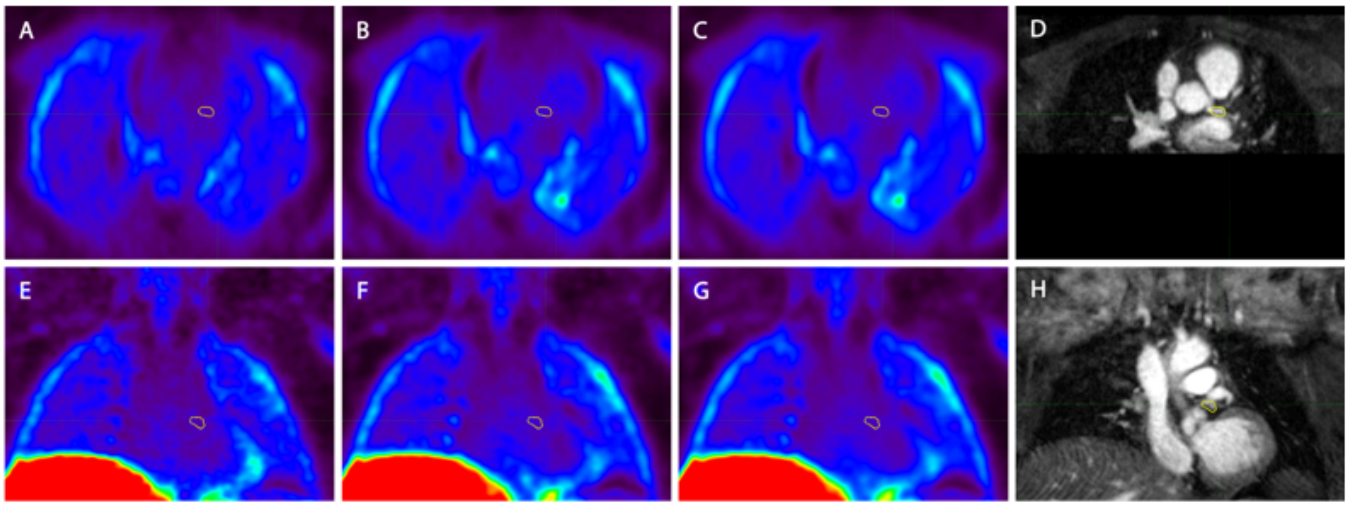

Figure 4

Example of the three different PET reconstructions in one patient (A and E: standard multigate respiratory gating motion correction (MRG-MOCO), B and F: extended MR-based motion correction (eMR-MOCO), C and G: extended MR-based motion correction with ECG gating (eMR-MOCO-ECG)), accompanied by 2D image-navigator-based motion-corrected 3D whole-heart MRI for anatomical reference (D and H). The top row images show axial reconstructions while the bottom row shows coronal reconstructions. The yellow volume of interest (VOI) was drawn over the main branch of the left coronary branch (A-H), which contains a vulnerable plaque. Within the VOI, no visually increased uptake was observed.

Supplementary Files

This is a list of supplementary files associated with this preprint. Click to download.

- GraphicalAbstract.png